Data S1 Inventory

This PDF file includes: 1) a detailed description of the procedures to calibrate the mechanical model using flexural rigidity measured from bending MTs and elasticity constant measured from denting MTs with AFM, 2) a detailed description of procedures for choose model parameters and an extensive sensitivity analysis of model parameters.

Data S1

Details on calibrating mechanical model using flexural rigidity. There are two types of experimental measurements of the flexural rigidity (*EI*) of MTs. One infers *EI* from thermal fluctuations MTs, the other uses mechanical force to bend MTs and extract *EI*. To simulate the former, there is too much uncertainty on what parameters should be used to characterize the thermal noise in the environment, partially due to the complex buffer solutions used to prepare MTs. In addition, computational cost associated with simulating thermal fluctuations is also too high. Therefore, we simulated bending of MTs to calibrate our model parameters using *EI* from experimental measurements.

In simulation of the bending of a MT, we used a MT of 200 rows of dimers. We start with the relaxed MT and shorten the distance between the two ends gradually (1 nm at each step) so that the MT gradually arches up. At each step, we used L-BFGS method to minimize the energy of the system. We also extracted the arch *s* that traces through the center of the MT by averaging over the 13 arches that tracing the 13 PFs. With this arch, we can compute the elastic energy stored in the MT using the formula:

$$U(s) = \frac{1}{2} EI \int_0^{l(s)} \frac{ds}{R^2(s)}$$

Here, $U(s)$ is the elastic energy stored in the MT, EI is the experimentally measured flexural rigidity, $l(s)$ is the length of the arch *s*, $R(s)$ is the radius of curvature at position s along the arch. Using *s* extracted from simulation, we can compute $R(s)$ and the integral.

Using EI from experimental measurement, we can compute $U(s)$. At the same time, $U(s)$ can also be computed using our mechanical model. We tuned the parameters in our mechanical model so that $U(s)$ calculated from the mechanical model matches the value calculated using the equation above (S4). In this way, we use our mechanical model to reproduce the experimentally measured EI. As a check, we also examined the relationship between $U(s)$ computed with our mechanical model and $\int_0^{l(s)} \frac{ds}{R^2(s)}$, and found that the relationship is linear. This confirms that our mechanical model produces a well-defined flexural rigidity.

We also tried shorter MT with 100 rows dimer and found the that the value of *EI* from our model is independent of the length of the MT and the extent to which we bend the MT. We were not able to simulate a MT of the same length as used in experiment because of the computational cost associated with energy minimization. On the other hand, our simulation does not suffer from the thermal fluctuations that could make a longer MT appear to have lower flexural rigidity that experiments have. In the end, our target is to have a mechanical model that can reproduce a flexural rigidity that we considered as reliable, not to reproduce experimental process.

From the calibration process, we found that the flexural rigidity is mainly determined by k_{long}, the force constant for the stretching of longitudinal bonds, but is insensitive to the other parameters. Therefore, flexural rigidity mostly calibrates k_{long} but imposes little constraints on the other parameters. Physically, this result is not surprising because the bending used in experimental measurement of flexural rigidity only distort the MT along the MT axis and it is on a length scale much larger than the inter-monomer distance. Therefore, the microscopic change needed to produce this macroscopic distortion is the stretching of the inter-monomer distance. For instance, the bending in longitudinal bond required to produce this macroscopic curvature is minimal. We picked a k_{long} value that gives $EI = 1.8 \times 10^{-24} N \cdot m^2$, the value for taxol-stabilized MTs measured in refs. (Kikumoto et al., 2006, Felgner et al., 1996). We pick the flexural rigidity of taxol-stabilized MTs because they are structurally similar to MTs of GMPCPP tubulins, which mimics the properties of MTs of GTP tubulins. The mechanical model was intended to handle mechanical energy in sheet structures, which are composed of GTP tubulins.

Details on calibrating mechanical model using AFM denting. In denting experiment, an AFM tip with a radius of ~20 nm was pressed against the MT wall. The force on the AFM tip and the indentation (measured as the vertical displacement of the AFM tip) shows a linear relationship, from which a spring constant that characterizes the elastic response of the MT wall is extracted. For calibration purpose, our target is to use our mechanical model to reproduce experimentally measured spring constant.

In our simulation, we have a MT of 50 rows fixed to a surface by fixing 3 PFs at the bottom so that the MT will not roll. The interactions between the AFM tip and the tubulins monomers were

modeled using the purely repulsive part of the WCA potential with the minimum lifted to 0 to mimic hard sphere interactions. The radius of the AFM tip is set to 20 nm and the radius of the tubulin monomers is 2 nm.

We started with the AFM tip touching the wall but not exerting any discernable force on the MT. We then gradually move the AFM tip downward vertically, 0.2 nm at each step. After each movement of the AFM tip, we minimize the energy of the MT using L-BFGS algorithm. The force on the AFM tip is computed, which is the sum of the forces between the AFM tip and all the tubulin monomers, which basically include only those that are in touch with it due to the hard sphere nature of their interactions. The vertical component of this force, which is very close to the total force (~98%), is plotted against the vertical displacement of the AFM tip in the range between 0 and 4 nm, which gives a linear relationship. From the slope of this linear relationship, we extract the spring constant k of the MT wall. We adjusted parameters in our mechanical model so that the spring constant from our simulation matches the experimentally measured value 0.08 N/m in ref. (de Pablo et al., 2003, Schaap et al., 2006).

As a check, we also plotted the total elastic energy in the MT computed from our mechanical model and plotted it against the vertical displacement of the AFM tip. We found a quadratic relationship, from which we can extract a spring constant as well. This spring constant has the same value as the spring constant extracted from the force-displacement relation. We also tried AFM tip with a radius of 30 nm and got the same results.

We found that the denting result is mostly sensitive to k_α, the spring constant for lateral bond rotation, in line with the results from Wu et al. The value of k_α from simulation is very similar to their value, even though they have an extra term for sliding between neighboring PFs in their mechanical model that has overlapping effects with the lateral bond bending term.

Other constraint used in determining the mechanical model. While the flexural rigidity and denting simulations calibrated k_{long} and k_α, they impose little constraints on the other parameters. Among these two, k_{long} contribute little to mechanical energy during sheet-to-tube transition, whereas k_α is important. This not surprising as the longitudinal twisting is the only longitudinal

term that is involved in the geometric mismatch between tubulins in B and S forms.

On the other hand, the purpose of the mechanical model is to capture the mechanical energy involved in the sheet-to-tube transition during growth. A process most relevant to this is the intriguing observation by Wang and Nogales that the cold-stable sheet of GMPCPP tubulins can spontaneously convert into tubes upon increasing temperature. We computed the mechanical energy profile for the conversion of a full 13-PF sheet of 30 rows into a tube by systematically going through B→S transition of each dimer one by one and row by row. One example of such a profile is shown in Fig. S6. We kept the values of k_{long} and k_{α} to be those calibrated by flexural rigidity and denting simulations and adjusted the other parameters to make sure that the height of the mechanical profile is in the range between 40 kT and 60 kT. This is because the mechanical energy profile shown in Fig. S6 is closely correlated to the mechanical energy profile encountered by the system during a temperature-induced sheet-to-tube conversion. Based on our basic understanding of reaction dynamics and kinetics, the mechanical energy barrier for the temperature-induced sheet-to-tube conversion cannot be too high or too low. If it is too high, sheet-to-tube transition will not be possible. If it is too low, tube will be the preferred stable structure even at low temperature. This requirement imposed quite tight general constraints on all the parameters important to sheet-to-tube transition—the twisting of longitudinal bond and stretching of lateral bonds (i.e. k_{ϕ} and k_{lat}).

Choice of model parameters and sensitivity analysis. Our model provided molecular mechanisms for the important phenomena of dynamic instability (i.e. catastrophe, rescue, shortening, pausing, sheet phase) at both plus and minus ends from a unified view. The core of these mechanisms are the kinetic pathways for the corresponding conformational changes, which are the pathways with minimum energy barriers based on the general theory of conformational dynamics (Boehr et al., 2009, Henzler-Wildman and Kern, 2007, Kumar et al., 2000). Therefore, the most essential parameters in our model are the energies of different conformational states. These conformational states are basins in the free energy landscape of microtubule, and their energies are the depths of their corresponding basins. Therefore, these parameters have specific and clear physical meaning. However, no attempts have been made to measure these conformational states of tubulin and their energies by the proper experimental techniques, such as

NMR relaxation dispersion. We have to choose the values for these energies based on related though indirect experimental information and relevant physical principles, as listed below.

1. The steric rules that we inferred and summarized from existing structural data provides the relative ranking of the energies of different conformational states on a kinetic pathway.

2. The tubulin conformational changes in our model are similar to the tier 0 conformational dynamics (Henzler-Wildman and Kern, 2007) studied extensively using smFRET technique in many protein systems over the past 20 years. These experiments usually report the histograms of multiple conformations (Hanson et al., 2007, Lerner et al., 2018). From these data, the general observation was that the difference in free energy between conformations that inter-convert with each other are within a few k_BT, where T is temperature and k_B is the Boltzmann constant. Therefore, we chose our parameters such that the energy difference between two neighboring states on a kinetic pathway less than 4 k_BT (Figs. S5,7,10).

3. We determined the reaction rate constant for transition between two conformations using their free energies based on the linear free energy relationship (Fersht, 1998), which was widely used for similar situations in many areas of physical chemistry and molecular biophysics.

4. Under the constraints of the guidelines discussed above, we tuned these energy parameters to reproduce: 1) the kinetic parameters of dynamic instability reported by Walker et al (Walker et al., 1988), and 2) the existence of sheet structures during growth phase over a range of tubulin concentrations reported by Chretien et al (Chretien et al., 1995).

5. Other parameters in our model, such as rates for association, hydrolysis, and mechanical energy parameters, are similar to parameters used in other models in the literature. They were determined following the same procedure used by other models.

In our model, all the phenomena of dynamic instability (e.g. catastrophe, rescue) depend on a common set of elementary processes, mainly the B→S→C transitions. Each phenomenon is affected by all the parameters that determine the conformational changes that it involves. At the

same time, the same conformational transition is involved in more than one phenomenon. Consequently, each parameter affects multiple phenomena.

We performed extensive tests on how our model parameters affect different phenomena. For each parameter, we changed its value by ± 1 to 2 $k_B T$ and examined how it changes the kinetics of all the different phenomena of dynamic instability. This procedure requires a large number of simulations, each one involves significant computational cost. To make the computational cost manageable, we used a small number of simulations (30) for each data point. Because we already constrained our parameter values to be within a few $k_B T$ in our tuning process based on the typical energy changes involved in protein conformational changes observed in smFRET experiments, a variation of 1 to 2 $k_B T$ is a large perturbation. Below we discuss, for each parameter, 1) the phenomena that it affects; 2) how it affects them and the reasons.

In each figure, the left panel shows how the rates of growth and shortening depend on a specific parameter. The color convention for the left panel is: 1) Orange: plus-end growth rate; 2) Red: plus-end shortening rate; 3) Light blue: minus-end growth rate; 4) Blue: minus-end shortening rate. The right panel shows how the frequencies for catastrophe and rescue depend on this parameter. The color convention for the right panel is: 1) Orange: plus-end catastrophe frequency; 2) Red: plus-end rescue frequency; 3) Light blue: minus-end catastrophe frequency; 4) Blue: minus-end rescue frequency. In cases where a parameter is only involved in plus/minus-end pathways, we only show results on plus/minus-end, because it has no effects on processes that are determined by minus/plus-end pathways.

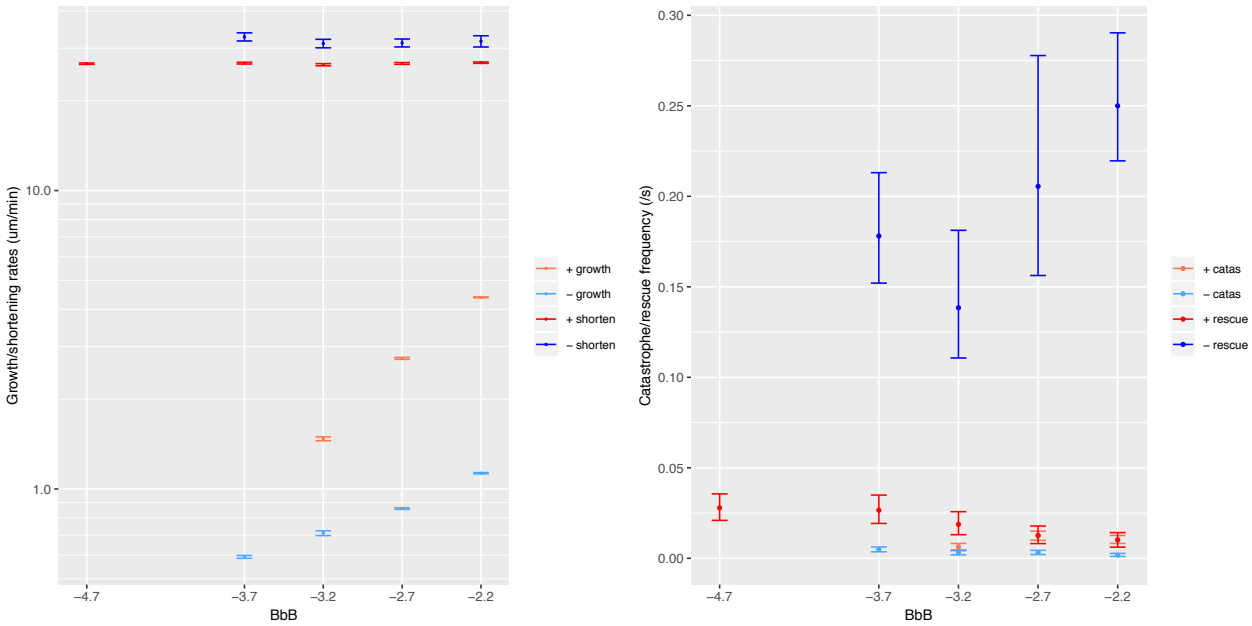

1) Energy of BbB (or B-b-B) interface. We were not able to decrease BbB energy significantly in simulations of growth and catastrophe due to computational cost, because it stabilizes BbB interface too much, leading to sheet structures that are too long. Simulation of sheet structure is computationally very expensive because it involves calculation of mechanical energy, which is much more expensive than kinetic simulations.

Increasing BbB energy increases plus-end growth because dimer dissociation decreases. This is because higher BbB energy accelerates B→S transition, which leads to shorter sheet phase and longer tube phase. Tube phase has less dimer dissociation because SsS and StS are more stable than BeB and BtB. Less sheet phase also leads to higher catastrophe frequency, because sheet structure prevent catastrophe.

Changing BbB energy has no effects on plus-end shortening, because it is determined by S→C transition whereas B→S transition is not involved. The BbB energy has little effect on rescue, because rescue involves dimer binding, thus B→S transition plays a small role in rescue due to many body effects.

At minus-end, increasing BbB energy also increases growth for the same reason as at plus-end, but the effects are much smaller because BbB plays a much smaller role in minus-end B→S

transition. It has very minor effects on catastrophe, because sheet structure has a much smaller role in preventing catastrophe at minus-end due to its much shorter lifetime. BbB energy has no effects on minus-end shortening because B→S transition is not involved. It has little effects on rescue for the same reason as at plus-end.

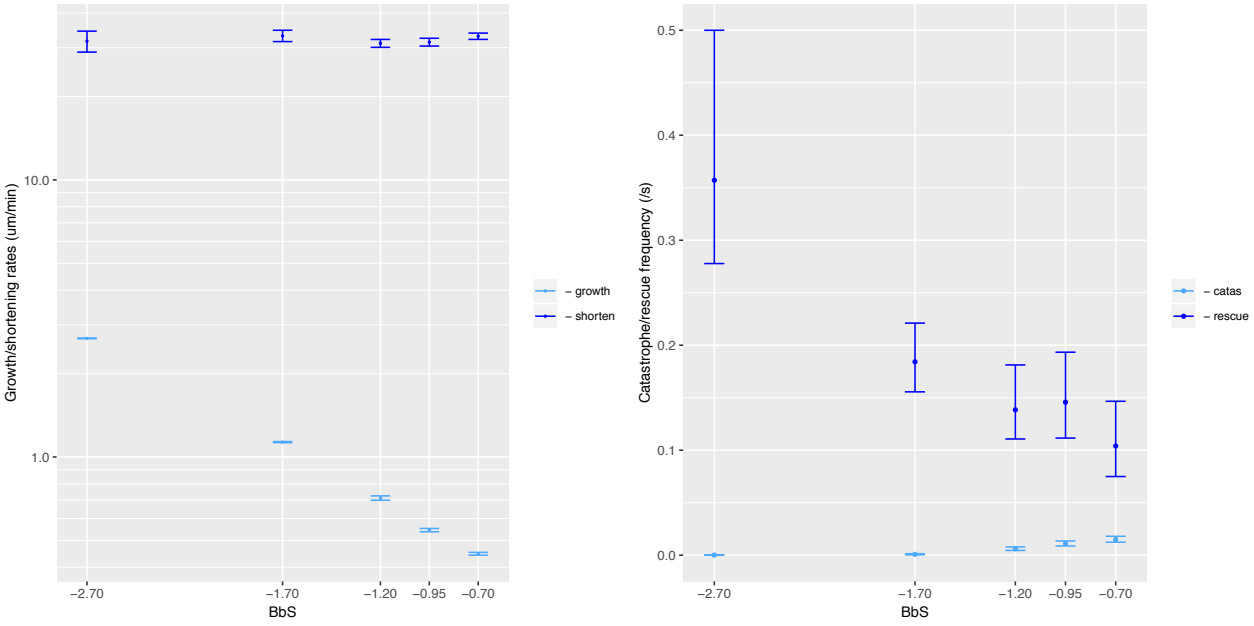

2) Energy of BbS (or B-b-S) interface. BbS energy has no effect on plus-end on plus-end dynamic instability because it is not involved in any plus-end pathways for B→S→C transitions.

At minus-end, decreasing BbS energy increases growth rate because it determines the dissociation rate at minus-end, thus stabilizing BbS interface decreases dissociation and consequently increases growth. Increasing BbS energy increases catastrophe because it makes growth slower, thus reducing its competition with S→C initiation, which makes catastrophe much easier. BbS energy has no effect on minus-end shortening because shortening is determined by S→C transition. In contrast, decreasing BbS energy increases rescue because it increases dimer addition after curved protofilaments break off by decreasing dimer dissociation.

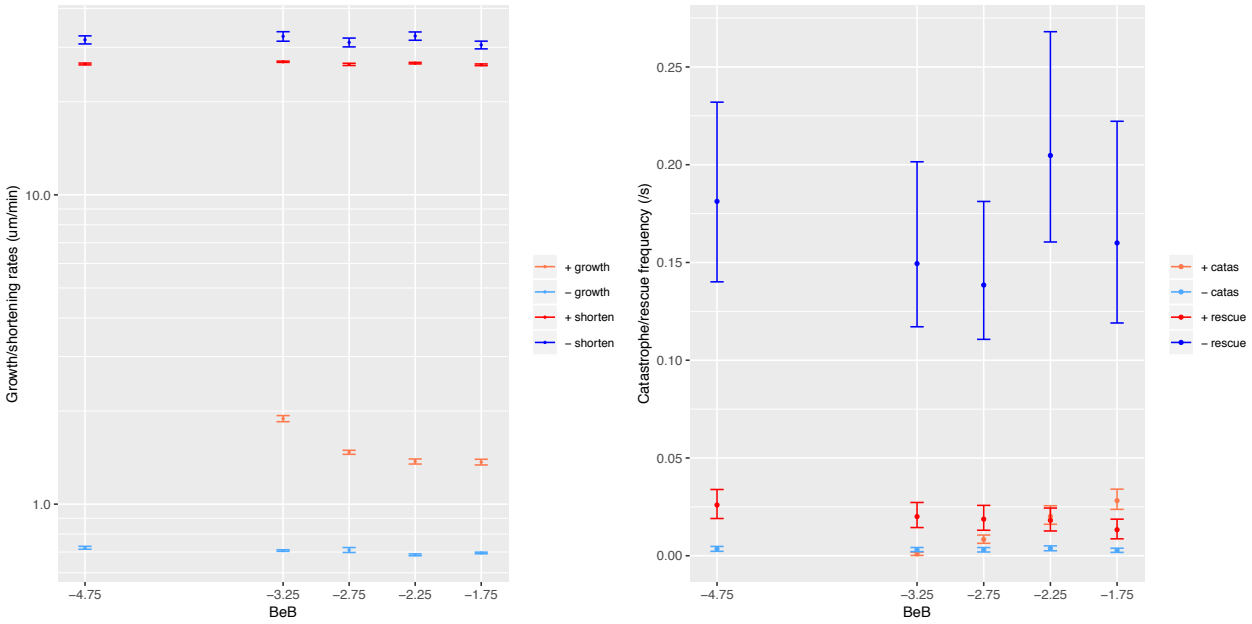

3) Energy of BeB interface. At plus-end, decreasing BeB energy slightly increases growth rate because it decreases dimer dissociation at BeB interface. But it also slows down B→S transition, thus its impact on growth rate is small because growth in sheet phase is slower than in tube phase. Prolonged sheet phase also decreases catastrophe because hydrolysis does not happen in sheet. It has not effect on shortening because shortening is determined by S→C transition alone. It has small effect on rescue due to is effect on dimer dissociation.

At minus-end, BeB energy has no effect on any aspects of dynamic instability because sheet has very short lifetime at minus-end.

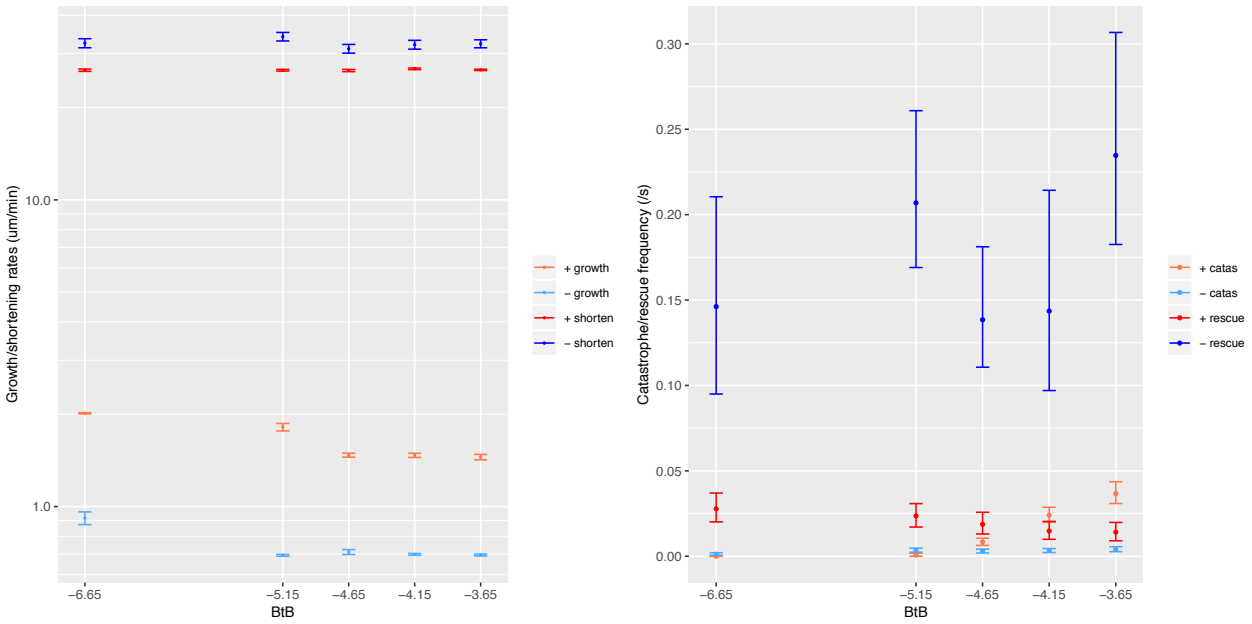

4) Energy of BtB interface. The effects of BtB energy on dynamic instability is very similar to those of BeB energy for the same reasons.

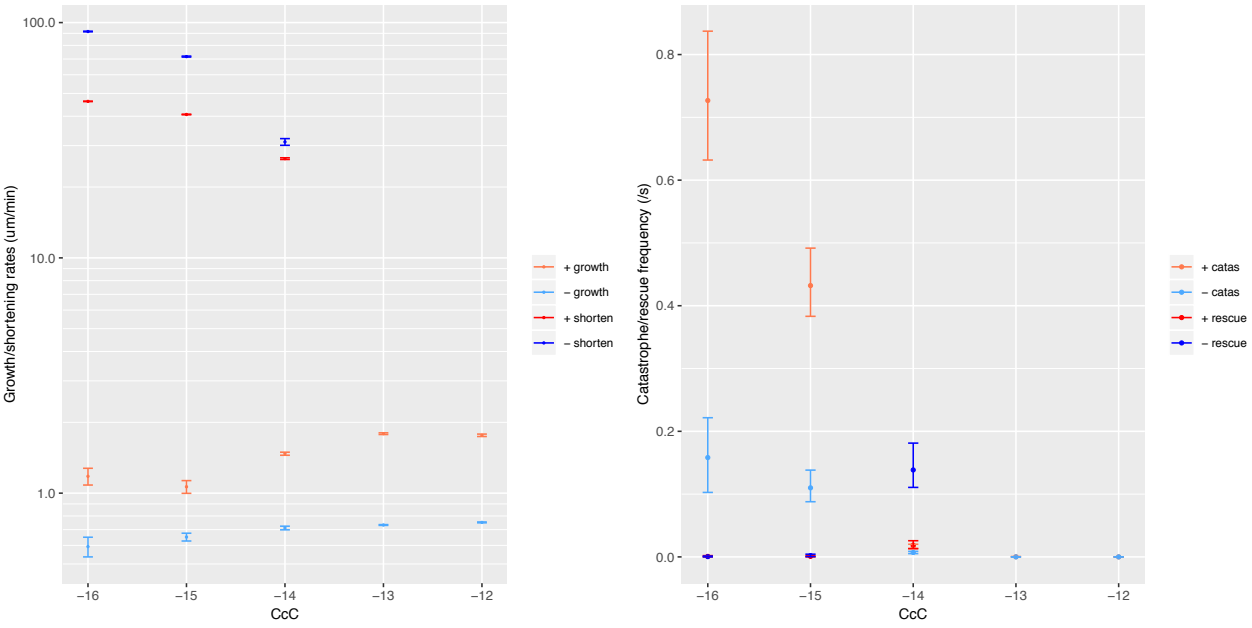

5) Energy of CcC interface. Decreasing CcC energy significantly increases catastrophe frequency and shortening rate and decreases rescue frequency because it makes S→C transition easy. Its effect on rescue is minor because rescue is more determined by dimer addition than S→C transition under this condition. At very high CcC energy, rescue happens too fast so that it is difficult and not meaningful to measure shortening rate and rescue frequency. Increasing CcC

energy increases plus-end growth rate slightly because it decreases number of curved protofilaments at growing plus-ends.

The CcC energy has similar effects on minus-end because it is the final state for S→C transition that is shared by both plus- and minus-ends.

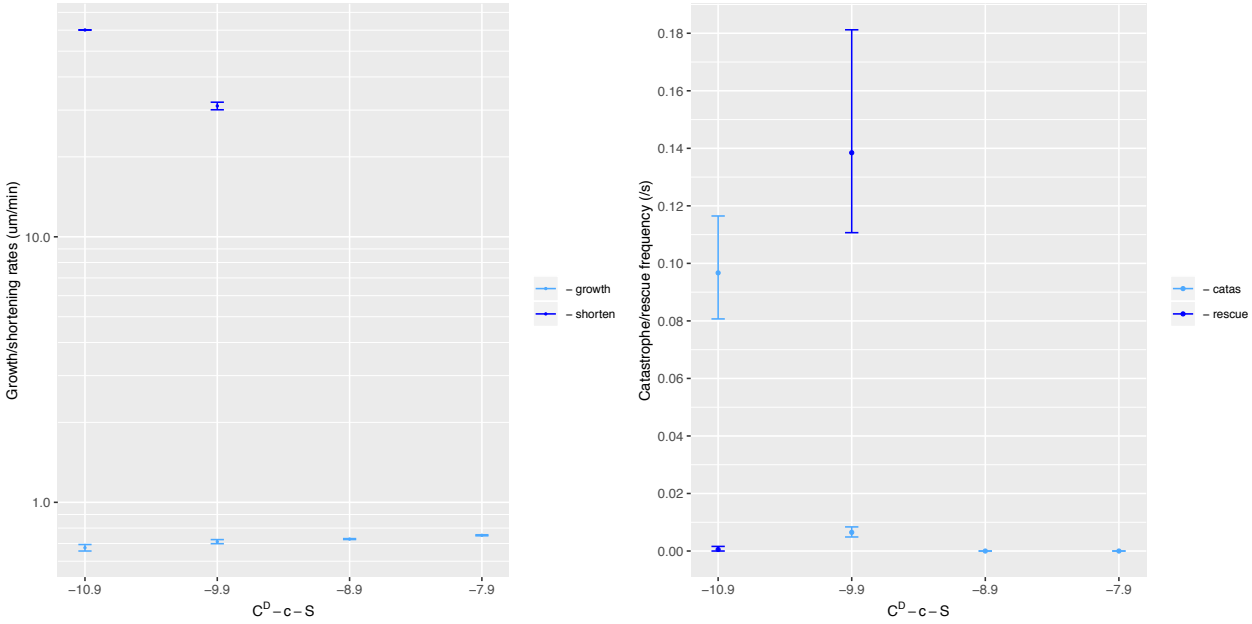

6) Energy of CcS interface. The CcS energy has no effects on plus-end dynamic instability because it is not on the kinetic pathways at the plus-end. At minus-end, decreasing CcS energy significantly increases catastrophe frequency and shortening rate and decreases rescue frequency because it makes S→C transition easy. At high CcS energy, a MT rescues immediately, thus it is not meaningful to calculate rescue frequency and shortening rate. Decreasing CcS energy also slightly decreases growth rate because it increases the number of curved protofilaments at growing minus-ends.

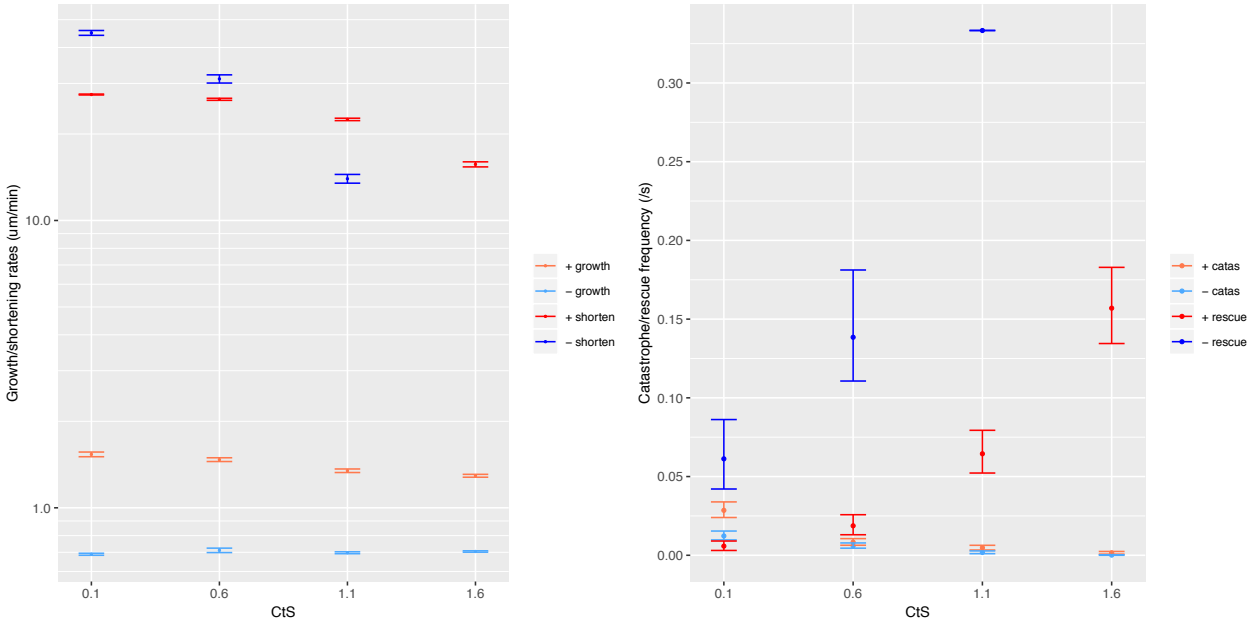

7) Energy of CtS interface. At plus-end, decreasing CtS energy increases growth rate slightly because curved protofilament has less impeding effects on dimer addition. It also increases catastrophe frequency and shortening rate because it enhances cooperative effects in S→C transition of neighboring dimers. It decreases rescue frequency for the same reason.

At minus-end, CtS energy has similar effects as at plus-end for the same reasons. These effects are slightly stronger due to the different topologies of the B→S→C transition pathways at the minus-end. For CtS energy at 1.6 kT, rescue happens too quickly, making it difficult to calculate rescue frequency and shortening rate in a meaningful way.

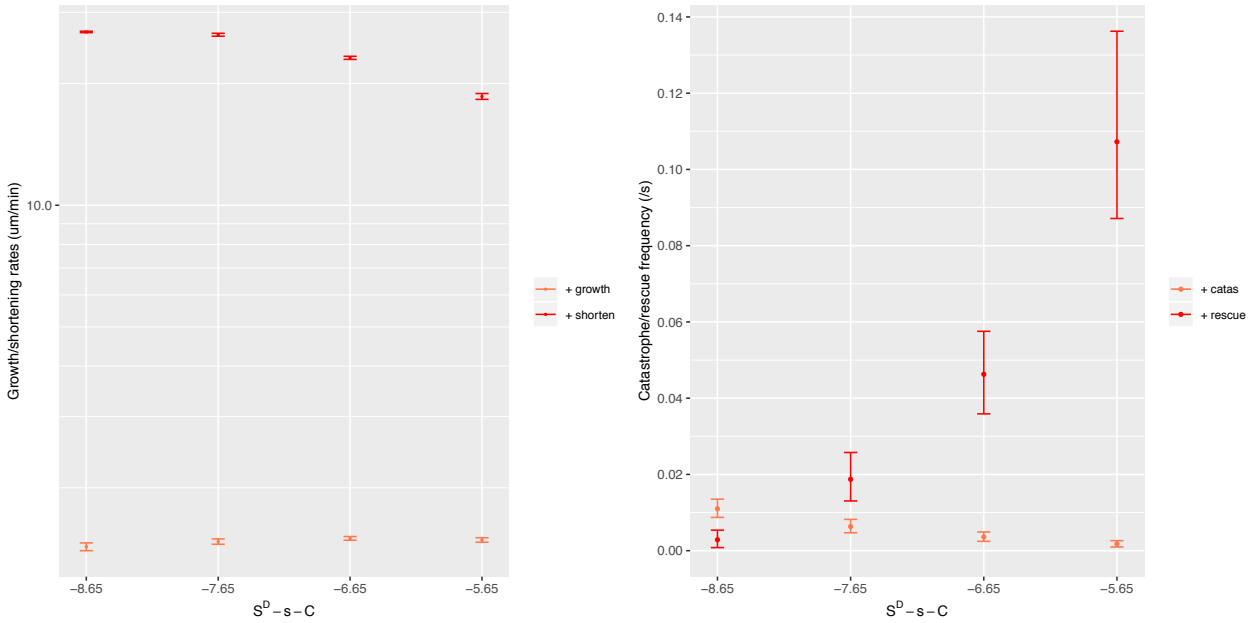

8) Energy of S^D-s-C interface. At the plus-end, S^D-s-C has no effects on growth because S→C transition is not involved in growth and S^D-s-C is not the end state of S→C transition, so that it has little effect on the number of curved protofilaments at growing plus-end, which is the way that S→C transition affects growth. On the other hand, decreasing S^D-s-C increases catastrophe frequency and shortening rate but decreases rescue frequency because it makes S→C transition easier. S^D-s-C does not affect minus-end dynamic instability because it is not on the minus-end kinetic pathways.

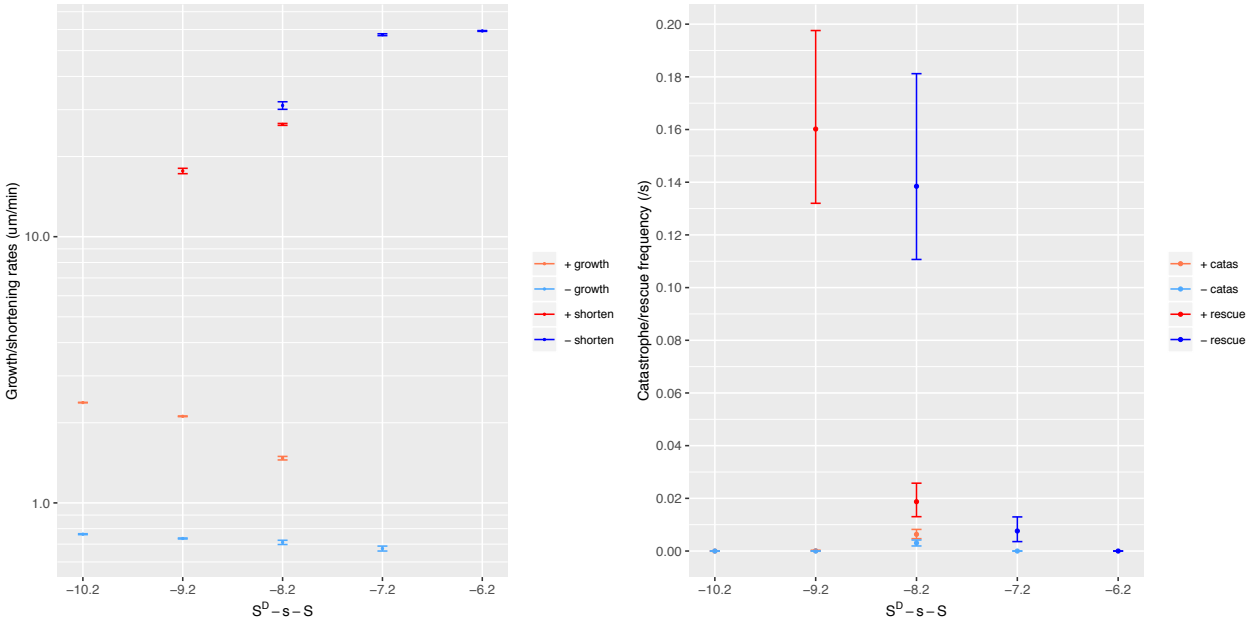

9) Energy of S^D-s-S interface. At plus-end, the energy of S^D-s-S interface is only scanned towards the more stable direction because otherwise it will become less stable than S^D-s-C interface, which will violate the steric rules. Decreasing S^D-s-S energy leads to more stable tube form, thus it leads to decrease in catastrophe frequency and shortening rate, and increase in rescue frequency. Stabilizing S^D-s-S interface also reduces the number of curved tip dimers at a growing plus-end, leading to slight increase in plus-end growth rate.

At minus-end, increasing S^D-s-S energy increases catastrophe frequency and shortening and decreases rescue frequency because it makes S→C transition easier. It also slightly increases growth rate as it decreases the number of curved tip dimers. At very low S^D-s-S energy, MTs do not really catastrophe or shorten, thus it is not meaningful to count rescue frequency.

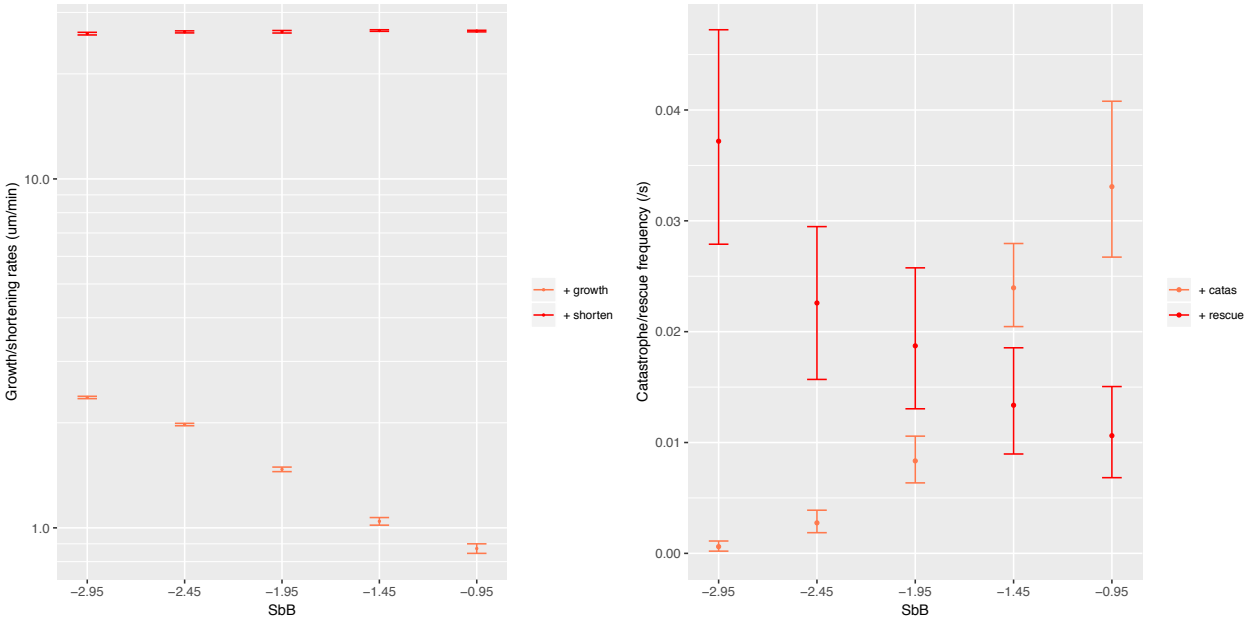

10) Energy of SbB (S-b-B) interface. Increasing SbB energy decreases plus-end growth rate because it leads to higher dimer dissociation at the S-b-B interface. It also increases catastrophe frequency because on average it reduces the length of sheet structure, which protects a plus-end from catastrophe. SbB energy has no effects on shortening rate because B→S transition is not involved in shortening. It has minor effects on rescue because it affects dimer association during

rescue. But dimer association during rescue is mostly in tube phase, making the impact of SbB very small.

SbB has no effects on minus-end dynamic instability because it is not on the kinetic pathway for B→S transition at minus-end. Although plus-end B→S pathway is not forbidden at minus-end, its energy cost is much higher than the optimal minus-end pathway, therefore minus-end B→S transitions do not follow this pathway.

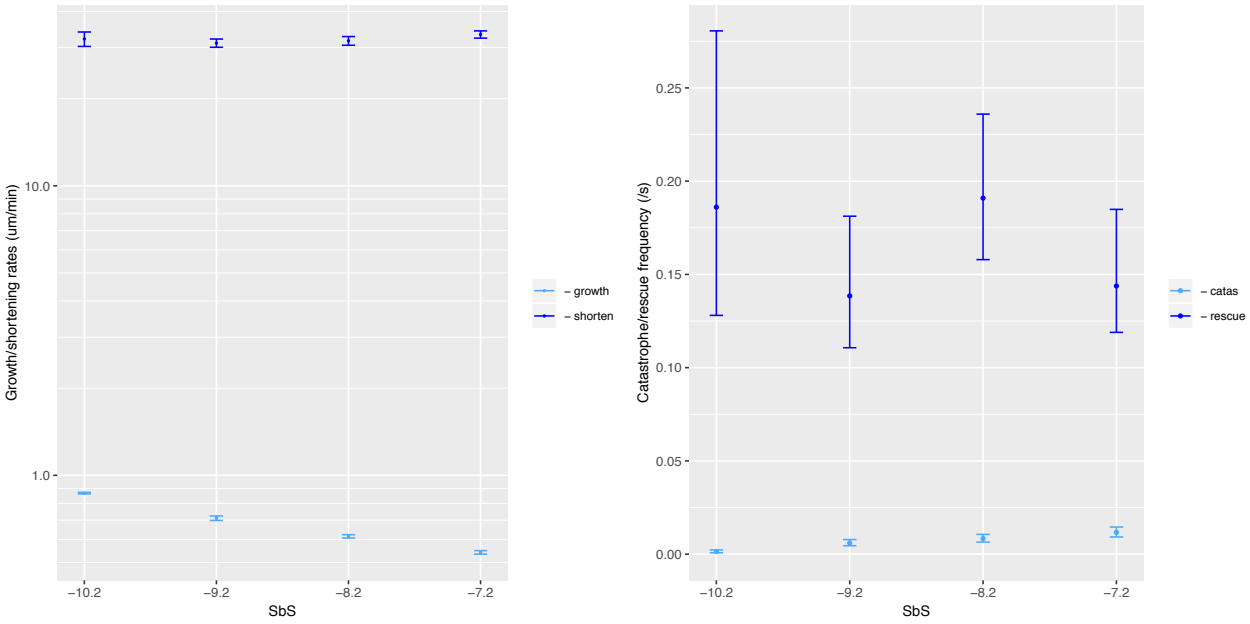

11) Energy of SbS interface. Energy of SbS has no effects on plus-end dynamic instability because it is not on the plus-end pathways for B→S→C transitions. Increasing SbS energy decreases minus-end growth rate because it makes B→S transition at minus-end more difficult, which effectively increases dimer dissociation at minus-end and therefore decreases growth. This decrease in growth also leads to increase in catastrophe, as catastrophe is determined by the competition between S→C initiation and dimer addition. Decreasing the latter without affecting the former leads to decrease in catastrophe. Changing SbS energy has no effect on shortening and rescue because they are mostly determined by S→C transition and SbS is not on the pathway of S→C transition.

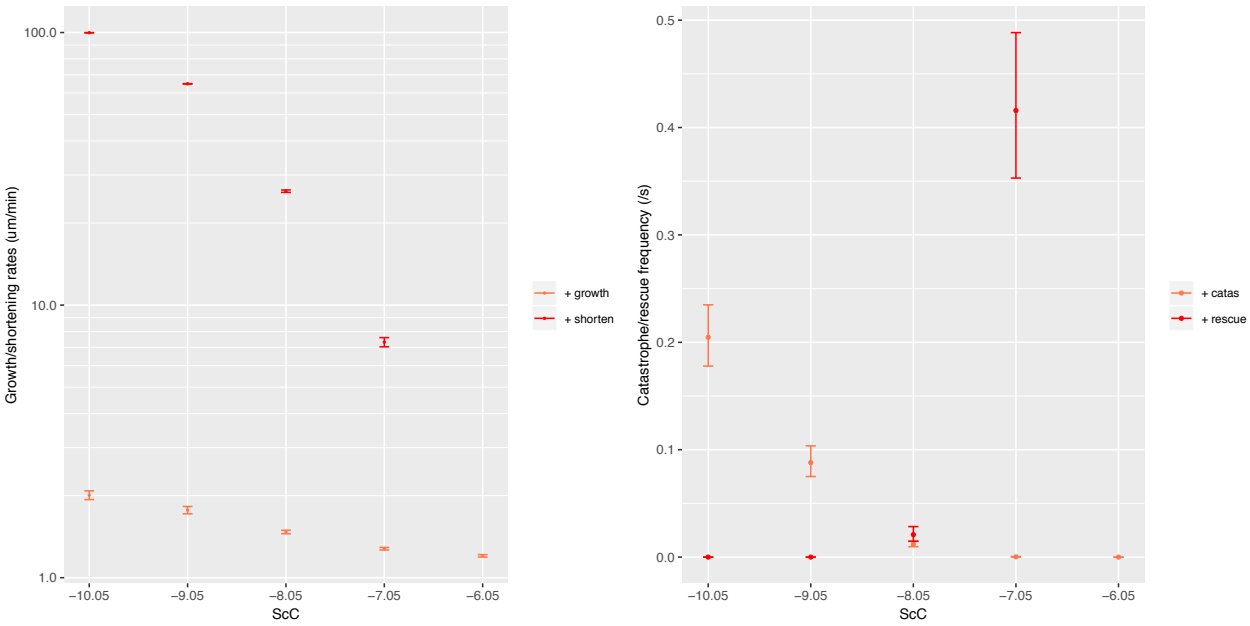

12) Energy of ScC interface. The ScC energy has no effect on minus-end dynamic instability because ScC interface is not on the minus-end pathways. Increasing ScC energy decreases catastrophe frequency and shortening rate significantly because it makes S→C transition more difficult, which is the determining factor for both catastrophe and shortening. For the same reason, it also increases rescue. Increasing ScC energy also leads to slight decrease in plus-end growth rate because it increases the number of partially curved tip dimers at a growing plus-end, which inhibit addition of new dimers to the tip. Increasing ScC energy does not change the S→C transition of the β-monomer of a tip dimer, but makes the next step, the SsC→ScC transition of the longitudinal interface more difficult. Thus it reduces the chance that a tip dimer fully converts into the C form. A curved tip dimer usually dissociates at the S-c-C interface. Without fully conversion into the C form, a partially curved tip dimer will not dissociate. This is the reason that increasing ScC energy alone actually increases the number of partially curved tip dimers, even though it decreases the overall S→C transition. This effect is small because a β-monomer in C form easily reverts to S form. Thus increasing ScC energy only leads to slight decrease in growth.

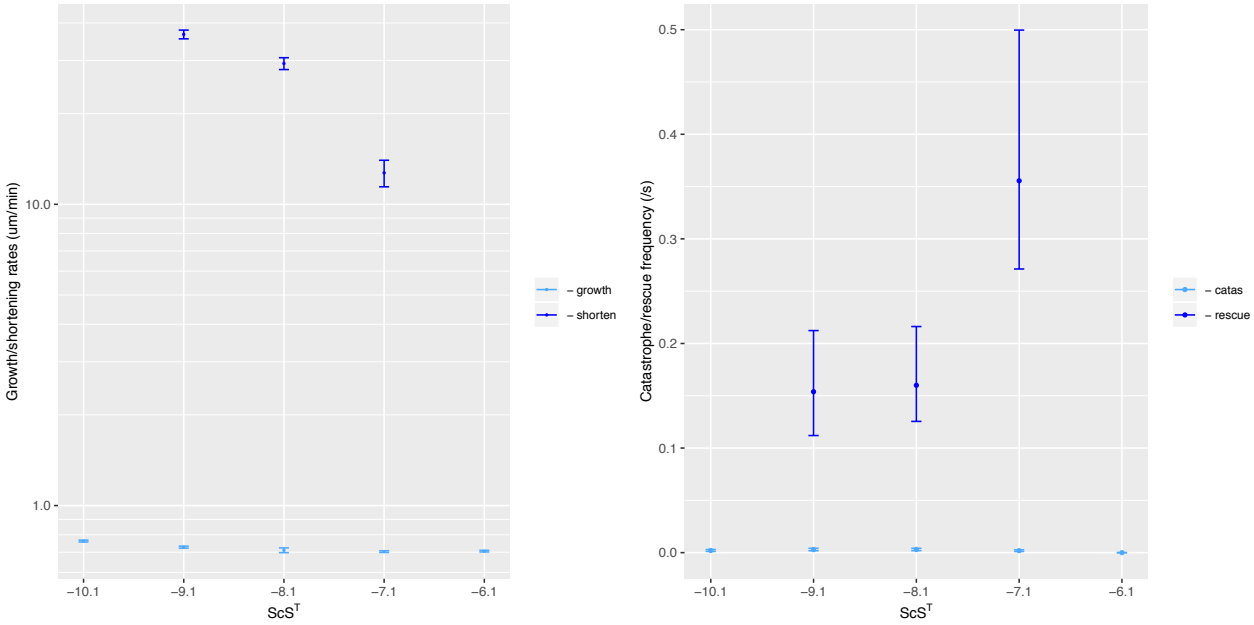

13) Energy of ScS^T interface. Increasing ScS^T energy decreases catastrophe frequency and shortening rate, and increases rescue frequency at minus-end, because it makes S→C transition more difficult at minus-end. It does not affect minus-end growth because S→C transition is not involved in growth. ScS^T energy does not affect plus-end dynamic instability because ScS interface is not on the plus-end pathways.

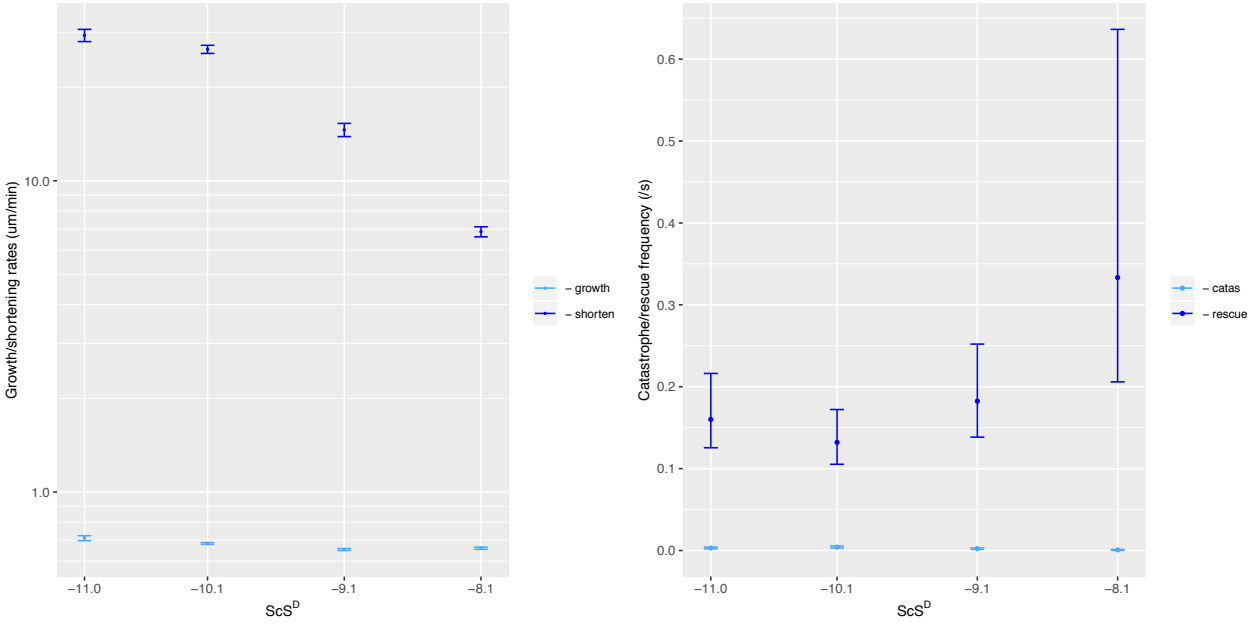

14) Energy of ScS^D interface. The energy of ScS^D interface has similar effects on minus-end dynamic instability as the energy of ScS interface does, because they play similar roles in the

minus-end S→C transition. Similarly, it does not affect plus-end dynamic instability because it is not involved in the plus-end pathways.

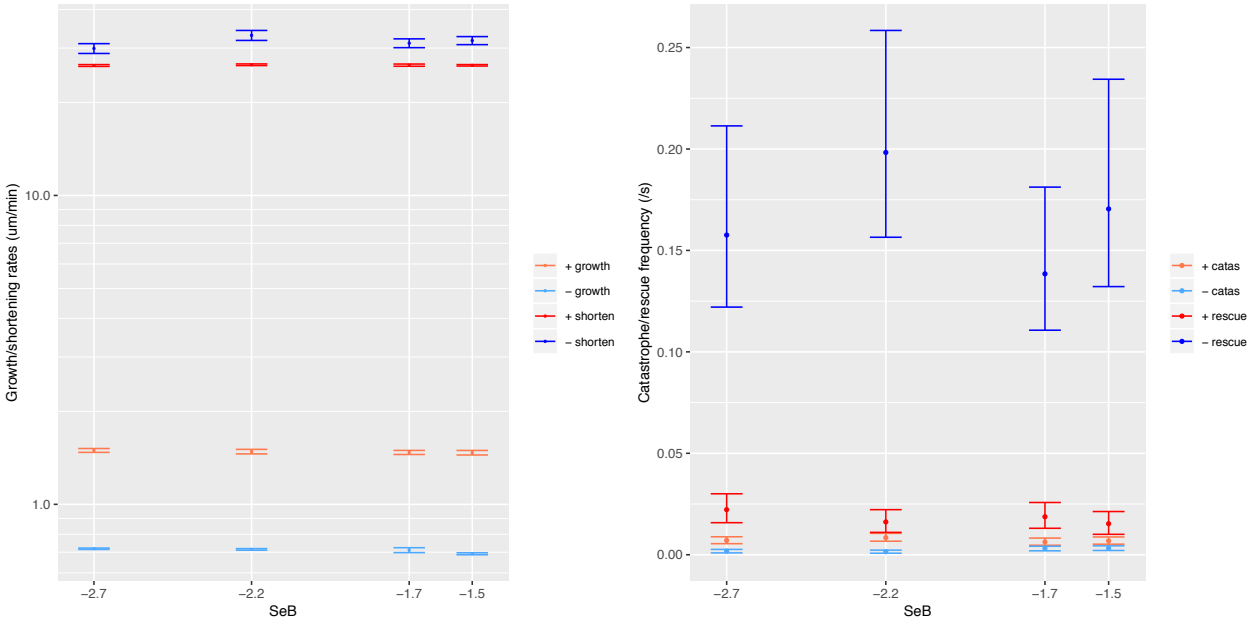

15) Energy of SeB interface. The energy of SeB interface has little effect on growth and catastrophe at either plus- or minus-end. The SeB interface appears on B→S pathway at both ends but plays a minor role, because SeB interface does not contribute to the major barrier for B→S transition. SeB does not affect shortening or rescue at either ends because these processes are determined by S→C transition, which does not involve SeB interface.

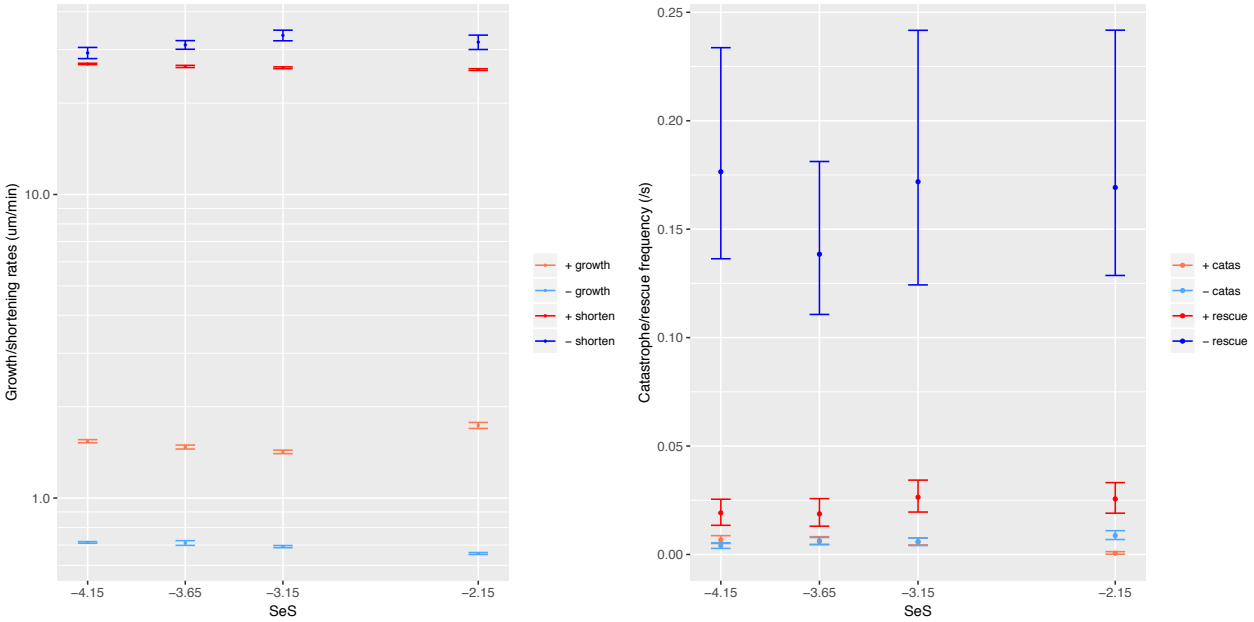

16) Energy of SeS interface. The energy of SeS has little effect on plus-end catastrophe until it becomes rather high (-2.15 k_BT). In this case, it significantly decreases catastrophe because it makes sheet closure slow, leading to long sheets at growing plus-end, which prevents catastrophe. It has little effect on growth rate because growth rates in tube and sheet phases are similar. It does not affect minus-end catastrophe because sheet phase is much more transient at minus-end, thus it does not affect catastrophe. The energy of SeS does not affect shortening and rescue at either end because these processes are determined by S→C transition, which does not involve SeS interface.

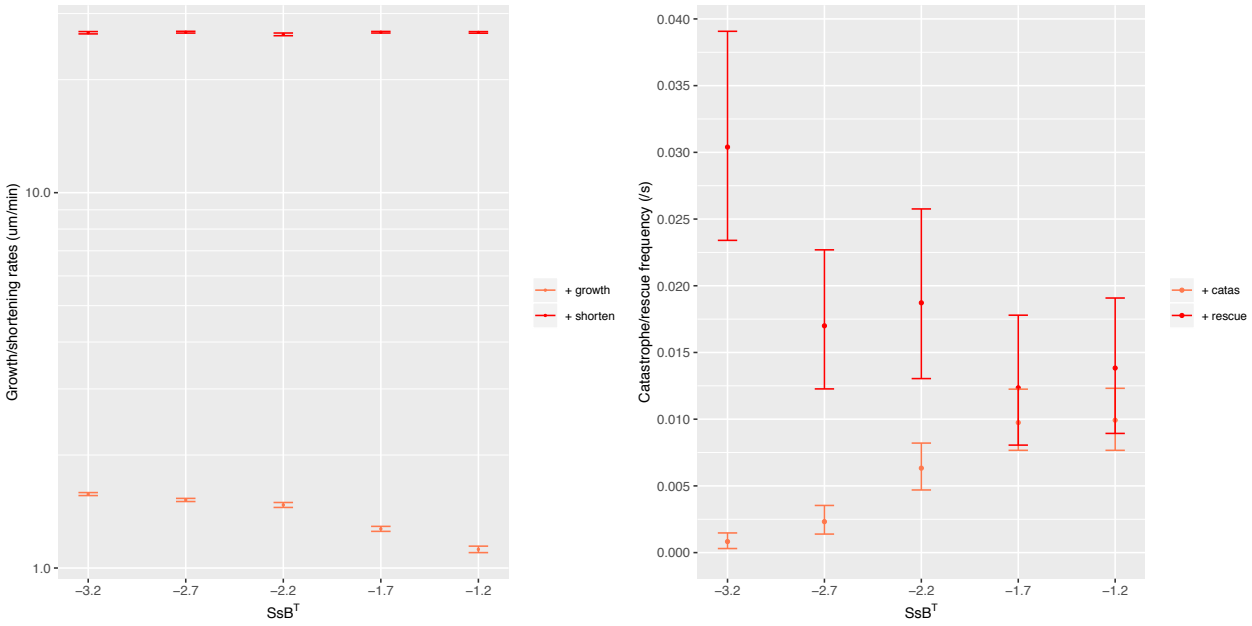

17) Energy of SsB^T interface. Increasing SsB^T energy decreases plus-end growth because it leads to higher dimer dissociation at the S-s-B interface. It also increases catastrophe because it reduces the length of sheet structure on average, which protects a plus-end from catastrophe. SsB^T energy has no effects on shortening rate because B→S transition is not involved in shortening. It has minor effects on rescue because it affects dimer association during rescue. But dimer association during rescue is mostly in tube phase, making the impact of SsB^T very small. SsB^T has no effects on minus-end dynamic instability because it is not on the pathway for B→S transition at minus-end.

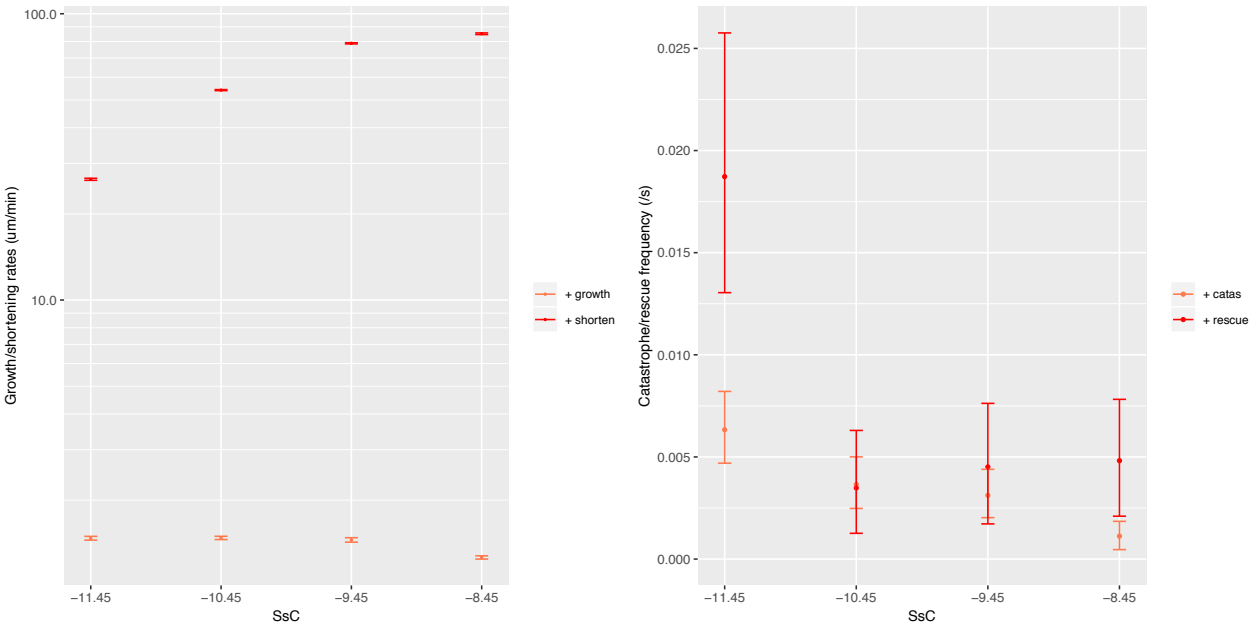

18) Energy of SsC interface. Increasing SsC energy decreases plus-end catastrophe frequency and shortening rate because it makes S→C transition more difficult. It decreases rescue frequency mildly because rescue is more determined by dimer addition and protofilament cleaving at ScC interface in this parameter regime. It does not affect growth because growth does not involve S→C transition. The energy of SsC interface has no effect on minus-end dynamic instability because it is not involved in minus-end pathways.

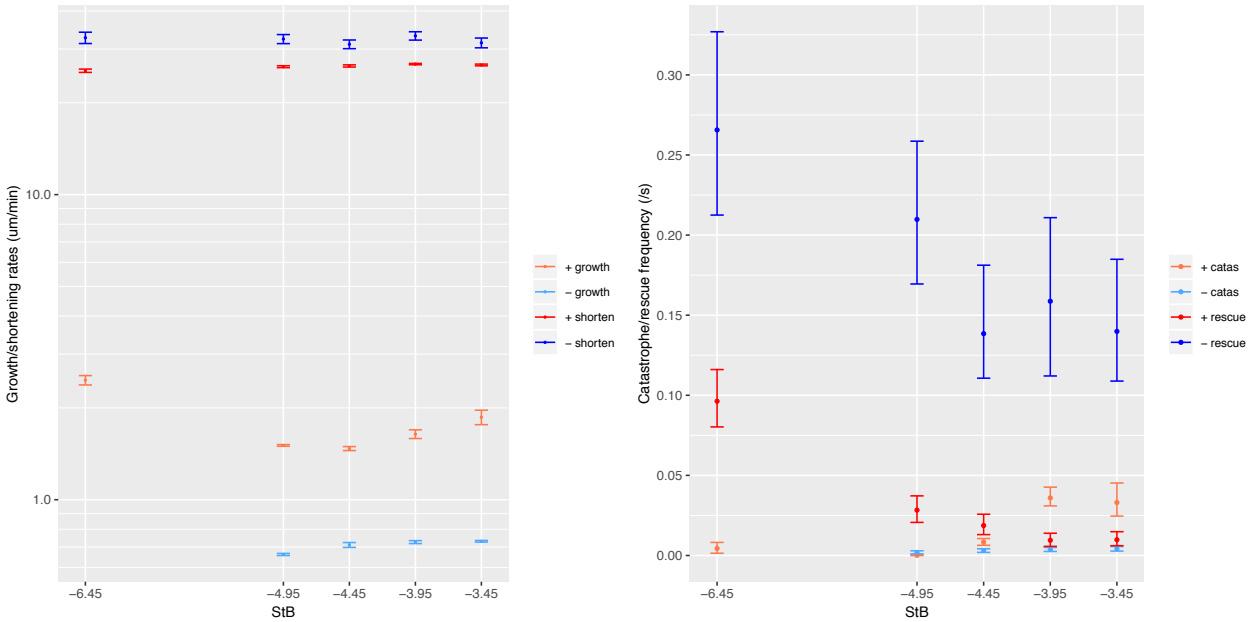

19) Energy of StB interface. The energy of StB has little effect on plus-end growth rate because two effects cancel with each other. On the one hand, more stable StB means dimer addition is

easier in tube phase. However, it also slows down B→S transition, which leads to prolonged sheet phase. Consequently, dimer additions mostly happen in sheet phase, diminishing the effect of StB energy on dimer addition, as StB mostly affects dimer additions to the sheet. Decreasing StB energy decreases catastrophe because it leads to longer sheet phase, which prevents catastrophe. It also increases rescue because it makes dimer addition to tube ends easier.

At minus-end, stabilizing StB interface decreases growth rate because it slows down B→S transition, which leads to more dimer dissociation at minus-end. At E(StB) = -6.45 k_BT, sheet structure forms at minus-end, making simulations too slow to finish, thus there was no data. Similar to plus-end, stabilizing StB interface decreases catastrophe at minus-end because it reduced the chance of S→C initiation, as dimers increasingly bind to and then dissociate from minus-end.

The StB energy does not affect shortening at either end because it does not affect S→C transition, which determines shortening.

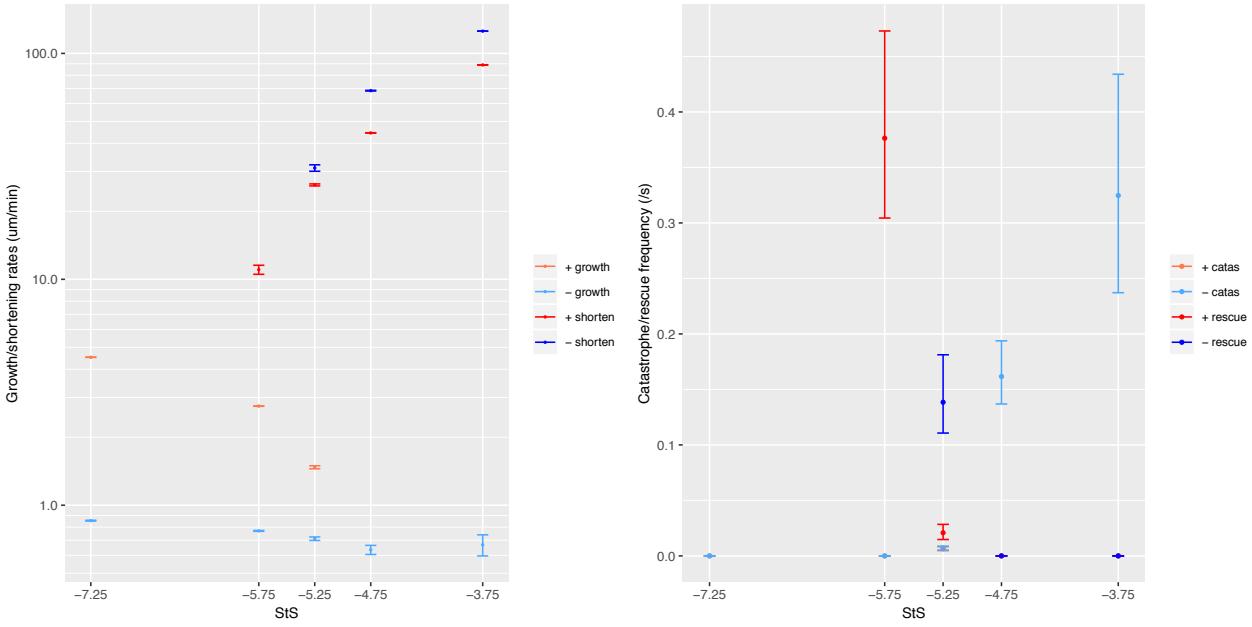

20) Energy of StS interface. The energy of StS interface affects dynamic instability at plus- and minus-ends in a similar manner, because it plays similar role in the B→S→C transitions at both ends. Increasing StS energy decreases growth rate and increases shortening rate because it destabilizes tube structure. For the same reason, it also increases catastrophe and decreases

rescue frequencies. At plus-end, when the StS energy reaches -4.75 k_BT or higher, dimers cannot straighten up fast enough so that the sheet grows too long, making simulations too costly to finish.

References

BOEHR, D. D., NUSSINOV, R. & WRIGHT, P. E. 2009. The role of dynamic conformational ensembles in biomolecular recognition. *Nat Chem Biol,* 5**,** 789-96.

CHRETIEN, D., FULLER, S. D. & KARSENTI, E. 1995. Structure of Growing Microtubule Ends - 2-Dimensional Sheets Close into Tubes at Variable Rates. *Journal of Cell Biology,* 129**,** 1311-1328.

DE PABLO, P. J., SCHAAP, I. A., MACKINTOSH, F. C. & SCHMIDT, C. F. 2003. Deformation and collapse of microtubules on the nanometer scale. *Phys Rev Lett,* 91**,** 098101.

FELGNER, H., FRANK, R. & SCHLIWA, M. 1996. Flexural rigidity of microtubules measured with the use of optical tweezers. *Journal of Cell Science,* 109**,** 509-516.

FERSHT, A. 1998. *Structure and mechanism in protein science: a guide to enzymer catalysis and protein folding,* New York, W. H. Freeman.

HANSON, J. A., DUDERSTADT, K., WATKINS, L. P., BHATTACHARYYA, S., BROKAW, J., CHU, J. W. & YANG, H. 2007. Illuminating the mechanistic roles of enzyme conformational dynamics. *Proc Natl Acad Sci U S A,* 104**,** 18055-60.

HENZLER-WILDMAN, K. & KERN, D. 2007. Dynamic personalities of proteins. *Nature,* 450**,** 964-72.

KIKUMOTO, M., KURACHI, M., TOSA, V. & TASHIRO, H. 2006. Flexural rigidity of individual microtubules measured by a buckling force with optical traps. *Biophys J,* 90**,** 1687-96.

KUMAR, S., MA, B. Y., TSAI, C. J., SINHA, N. & NUSSINOV, R. 2000. Folding and binding cascades: Dynamic landscapes and population shifts. *Protein Science,* 9**,** 10-19.

LERNER, E., CORDES, T., INGARGIOLA, A., ALHADID, Y., CHUNG, S., MICHALET, X. & WEISS, S. 2018. Toward dynamic structural biology: Two decades of single-molecule Forster resonance energy transfer. *Science,* 359.

SCHAAP, I. A. T., CARRASCO, C., DE PABLO, P. J., MACKINTOSH, F. C. & SCHMIDT, C. F. 2006. Elastic response, buckling, and instability of microtubules under radial indentation. *Biophysical Journal,* 91**,** 1521-1531.

WALKER, R. A., OBRIEN, E. T., PRYER, N. K., SOBOEIRO, M. F., VOTER, W. A., ERICKSON, H. P. & SALMON, E. D. 1988. Dynamic Instability of Individual Microtubules Analyzed by Video Light-Microscopy - Rate Constants and Transition Frequencies. *Journal of Cell Biology,* 107**,** 1437-1448.